e-ISSN: 2687-6698 **Research Article**

Turkish Journal of

Analytical Chemistry

TurkJAC

https://dergipark.org.tr/tr/pub/turkjac

Congo red removal from aqueous solution using 2-mercaptopropionic acid functionalized Fe_3O_4 magnetic nanoparticles

Ümit Can Erim

İstanbul Medipol University, School of Pharmacy, Department of Analytical Chemistry, 34815, İstanbul, Türkiye

Abstract

In this study, magnetic Fe_3O_4 nanoparticles were synthesized and were modified with 2-mercaptopropionic acid (MPA). This was done to enhance their adsorption performance toward Congo Red (CR) in aqueous solution. FTIR spectroscopy was used to characterize the resulting MPA-functionalized nanomaterial (Fe_3O_4@MPA), confirming the successful attachment of -SH and -COOH functional groups. To investigate the effects of pH, initial dye concentration, contact period and temperature, the batch adsorption technique was conducted. Since the adsorption capacity was not significantly affected by pH, pH adjustment was continued for minimal chemical and time savings. This finding indicates that the surface charge and functional groups of Fe_3O_4@MPA interact most favorably with CR molecules under near-neutral conditions. The adsorption data were fitted to isotherm models, and the optimal model was found to be the Langmuir model ($R^2 = 0.9901$), which shows single-layer adsorption with a maximum capacity of 120.48 mg/g. Analysis of the kinetic data revealed a correlation with the pseudo-second-order kinetic model, confirming the chemical adsorption mechanism with a determination coefficient (R^2) greater than 0.99. Thermodynamic parameters further confirmed the process to be spontaneous and endothermic, with negative $\Delta G°$, positive $\Delta H°$ (6.92 kJ/mol), and positive $\Delta S°$ (0.029 kJ/mol·K). More than 60% removal was achieved in real sample applications. This work presents a new approach using MPA-functionalized Fe_3O_4 nanoparticles, which both increases adsorption efficiency and magnetic recoverability, providing a sustainable and pH-independent method for Congo Red purification from real matrices.

Keywords: 2-Mercaptopropionic acid, adsorption isotherms, congo red, magnetic nanoparticles

1. Introduction

Synthetic dyes find extensive application across various industries, including textiles, plastics, and paper processing. Congo Red (CR) is an anionic azo dye formed from benzidine and exhibits significantly higher chemical stability compared to other dyes. The color is exceptionally vibrant, and it does not degrade naturally [1]. The accidental introduction of CR waste into aquatic systems significantly affects public health and the sustainability of the environment. Even minimal levels that are around the maximum residue level (MRL) value of CR can lead to the inhibition of photosynthesis, disruption of aquatic ecosystems, and an increased risk of cancer and genetic alterations in humans [1]. Due to its structure, comprising sulfonate chains and azo linkages, it exhibits increased solubility and persistence in aquatic environments, thereby complicating the processing efforts of wastewater treatment plants [2]. To address this issue, researchers have employed many conventional techniques for dye removal, including coagulation-flocculation, chemical oxidation, membrane filtering, and biodegradation treatments [3–6]. Each approach has perks and drawbacks; however, multiple approaches are impractical due to financial, operational, or environmental constraints [7]. Oxidation procedures often need substantial energy and generate secondary pollutants [8]; membrane techniques are effective but can get fouled and are expensive to operate [9]; biological treatments are not consistently effective against persistent dyes such as CR [10]. Conversely, adsorption has emerged as a favored strategy due to its simplicity, cost-effectiveness, efficacy at low concentrations, and applicability over a broad spectrum of pH levels. Moreover, adsorbents are frequently capable of regeneration and reuse, hence improving the sustainability of the process [11].

Citation: Ü.C. Erim, Congo red removal from aqueous solution using 2-mercaptopropionic acid functionalized Fe_3O_4 magnetic nanoparticles, Turk J Anal Chem, 7(3), 2025, 361–369.

***Author of correspondence:** uc.erim@gmail.com
Tel: +90 (0216) 444 85 44 **Fax:** +90 (212) 521 23 77
Received: August 16, 2025 **Accepted:** September 10, 2025
https://doi.org/10.51435/turkjac.1766160

Among the diverse array of adsorbents investigated, nanostructured materials, especially magnetic nanoparticles (MNPs) have garnered significant interest. Iron oxide (Fe_3O_4) nanoparticles are particularly appealing because of their superparamagnetic characteristics, chemical stability, elevated surface area, and ease of separation from aqueous solutions using external magnetic fields [12]. Nonetheless, uncoated Fe_3O_4 particles frequently agglomerate due to magnetic dipole–dipole interactions and typically lack the functional groups necessary for selective dye interaction. Surface modification procedures have been devised to include certain functional groups that augment dye adsorption and promote colloidal stability [13,14]. One functionalizing agent is 2-mercaptopropionic acid (2-MPA), a diminutive bifunctional molecule including both carboxylic (-COOH) and thiol (-SH) groups [15]. These groups offer several active sites for electrostatic interactions, hydrogen bonding, metal coordination, and π–π interactions with dye molecules. In the context of CR removal, carboxyl groups enable robust binding to the dye's sulfonic acid groups through ion exchange or hydrogen bonding, while thiol groups enhance affinity via soft acid-soft base interactions or potential chelation with heavy metals or charged dye intermediates [15]. The incorporation of 2-MPA enhances the water dispersion stability of the nanoparticles and inhibits aggregation by providing a negative surface charge under suitable pH settings [16].

This work involved the synthesis of 2-mercaptopropionic acid-functionalized Fe_3O_4 magnetic nanoparticles, which were utilized as an effective adsorbent for the extraction of CR from aqueous solutions. The influence of critical process variables such as pH, contact duration and starting dye concentration were methodically examined to enhance adsorption efficacy. The adsorption behavior was assessed by linear isotherm models (Langmuir, Freundlich, Temkin and Dubinin–Radushkevich), kinetic modeling was conducted using pseudo-first order, pseudo-second order equations and thermodynamic parameters were examined. In the adsorption tests, real wastewater treatment plant samples were used as matrix and the matrix effect was determined by adding certain concentrations of CR to these wastewaters. The results provide significant insight into the practical use of functionalized magnetic nanoparticles for the sustainable remediation of dye-contaminated effluents.

2. Materials and methods

2.1. Chemicals and instrumentation

All chemicals and solvents utilized in the study were of analytical grade and were used without further purification. 2-Mercaptopropionic acid (2-MPA), CR, HCl, NaOH, iron (III) chloride hexahydrate ($FeCl_3{\cdot}6H_2O$), iron (II) sulfate heptahydrate ($FeSO_4{\cdot}7H_2O$), and ammonium hydroxide solution (NH_4OH, 25%) were obtained from Sigma-Aldrich (Darmstadt, Germany). Deionized water produced using an ELGA PureLab system (High Wycombe, United Kingdom) was utilized throughout the experimental procedures, including solution preparation, nanoparticle synthesis, and cleaning steps. Dye concentrations were measured using a spectrophotometer (Shimadzu UV 1800, Japan) at a wavelength of 497 nanometers. All adsorption studies were conducted with (N-Biotek NB-T205, Korea) orbital shaker incubator at 200 rpm. pH measurements were conducted using a Mettler Toledo SevenCompact pH meter.

2.2. Preparation of working solutions

Stock solution was prepared from CR powder at 1000 mg/L concentration using ultrapure water. All working solutions were diluted from stock solution to obtain desired concentration of working solution in the volumetric flask.

2.3. Synthesis and surface modification of Fe_3O_4 nanoparticles

The synthesis of Fe_3O_4 magnetic nanoparticles was achieved via the chemical co-precipitation method. A solution was prepared by dissolving 5.4 g (20 mmol) of $FeCl_3{\cdot}6H_2O$ and 2.78 g (10 mmol) of $FeSO_4{\cdot}7H_2O$ in 100 mL of deoxygenated deionized water under a nitrogen atmosphere. The solution was subsequently heated to 80 °C while being stirred vigorously. Ammonium hydroxide (25%) was added incrementally until the pH reached 10. The black precipitate was separated using a neodymium magnet. The product was subsequently washed multiple times with deionized water and ethanol to ensure the removal of residual impurities. Subsequently, the precipitate was subjected to vacuum drying at 60 °C for 12 hours to ensure the complete removal of moisture and the formation of a solid material [17].

To achieve surface modification, 1.0 g of previously synthesized Fe_3O_4 was dispersed in 50 mL of ethanol via ultrasonication. Subsequently, 2.0 mL of 2-mercaptopropionic acid was added. The mixture underwent reflux at 70 °C for 12 hours. The modified nanoparticles (Fe_3O_4@MPA) have been collected utilizing a neodymium magnet, subsequently followed by several washes with ethanol and distilled water. The nanoparticles were subsequently dried in a vacuum oven [8,18].

2.4. FTIR characterization

The assessment of surface functional groups and chemical bonding pre- and post-surface modification was performed employing Fourier Transform Infrared Spectroscopy (FTIR). The spectra were acquired utilizing a PerkinElmer Spectrum Two FTIR spectrometer, covering the range of 4000–400 cm^{-1} at a resolution of 4.0 cm^{-1}.

2.5. Batch adsorption experiments

The pH level of the environment in which the adsorption process proceeds is a critical parameter to optimize. CR solutions were used at an initial concentration of 30 mg/L and adsorbent amount 10 mg to demonstrate the effect of pH. Solutions prepared at pH 4, 5, 6, 7, 8, 9, and without pH adjustment were mixed in an orbital shaker at 200 RPM for 2 hours to ensure equilibrium of adsorption and the absorbance of the solutions was read on a UV-VIS spectrophotometer. Acidity of the solutions were adjusted with 0.1 M HCl and 0.1 M NaOH until desired pH was obtained. An external magnetic field (neodymium magnet) was used to separate the synthesized magnetic adsorbent from the solutions.

2.6. Adsorption capacity

In order to test the suitability of adsorption to isotherm models, CR solutions with different initial concentrations (20, 30, 40, 80, 100 mg/L) were used, the concentration change occurring during the equilibrium period was recorded, and the adsorption capacities at different times and the adsorption capacity at equilibrium were calculated as follows,

$$q_t = (C_0 - C_e).V/W \quad (1)$$

where, V is the volume of the analyte solution (L); C_0 represents the initial concentration of CR (mg/L), and C_e is the equilibrium concentration after adsorption (mg/L). W denotes the weight of the adsorbent used (g) [19].

The experimental data obtained were evaluated using four commonly accepted adsorption isotherm models: Langmuir, Freundlich, Temkin, and Dubinin–Radushkevich (D–R). In order to facilitate parameter estimation and to assess model compatibility, the linear forms of these isotherms were used (Table 1). Linearization allows for easier graphical representation, straightforward determination of isotherm constants via linear regression [20]. Additionally, linear forms simplify the analysis and visualization of adsorption behavior over varying concentrations and allow for direct comparison of model performance using correlation coefficients (R^2) [21,22].

Table 1. Equations used for isotherm fittings

Isotherm Model	Linear Equation	Plot	Ref.
Langmuir	$C_e/q_e = C_e/q_{max} + 1/(K_L q_{max})$	C_e/q_e vs C_e	[23]
Freundlich	$\ln q_e = \ln K_F + 1/n \ln C_e$	$\ln q_e$ vs $\ln C_e$	[19]
Temkin	$q_e = B \ln A + B \ln C_e$	q_e vs $\ln C_e$	[24]
Dubinin–Radushkevich (D–R)	$\ln q_e = \ln q_m + \beta \varepsilon^2$ $\varepsilon = RT \ln(1 + 1/Ce)$	$\ln(q_e)$ vs ε^2	[25]

C_e: Equilibrium concentration (mg/L), q_e: Adsorbed amount at equilibrium (mg/g), q_{max}: Maximum adsorption capacity (mg/g), b: Langmuir constant related to adsorption energy (L/mg), K_F: Freundlich constant indicating adsorption capacity, $1/n$: Freundlich heterogeneity factor, A: Temkin binding constant (L/g), B: Constant related to heat of adsorption, B=RT/b_T, β: D–R constant related to adsorption energy (mol^2/J^2), ε: Polanyi potential, **R**: Universal gas constant (8.314 J/mol·K), **T**: Absolute temperature (K).

The use of these linearized equations enables not only the derivation of model parameters through simple slope-intercept calculations but also provides a reliable means to evaluate the appropriateness of each isotherm for the experimental system under study. Several recent studies have confirmed the relevance of these models in heavy metal and dye removal from aqueous solutions using various adsorbents, such as activated carbons, nanocomposites, and biochars [26–28].

To examine the adsorption process and rate-limiting steps of CR removal by Fe_3O_4@MPA nanoparticles, experimental findings were assessed utilizing two kinetic models: pseudo-first order (Eq. 2), pseudo-second order (Eq. 3). The studies were performed at various temperatures (30 °C, 40 °C, 50 °C, and 60 °C) and the adsorption capacity over time (q_t) was calculated over a period of 90 minutes.

$$\ln(q_e - q_t) = \ln q_e - k_1 t \quad (2)$$

$$t/q_e = 1/k_2 q_e^2 + t/q_e \quad (3)$$

The use of these linearized equations enables not only the derivation of model parameters through simple slope-intercept calculations but also provides a reliable means to evaluate the appropriateness of each isotherm for the experimental system under study. Several recent studies have confirmed the relevance of these models in heavy metal and dye removal from aqueous solutions using various adsorbents, such as activated carbons, nanocomposites, and biochars [26–28].

To examine the adsorption process and rate-limiting steps of CR removal by Fe_3O_4@MPA nanoparticles, experimental findings were assessed utilizing two kinetic models: pseudo-first order (Eq. 2), pseudo-second order (Eq. 3). The studies were performed at various temperatures (30 °C, 40 °C, 50 °C, and 60 °C) and the adsorption capacity over time (q_t) was calculated over a period of 90 minutes.

$$\Delta G^o = -RT \ln K \quad (4)$$

$$\ln K = \Delta S^o/R + \Delta H^o/RT \quad (5)$$

$$\ln k_2 = \ln A + E_a/RT \quad (6)$$

Where Ea (kJ/mol) is the activation energy, T (K) is the absolute temperature, R (J/mol.K) is the ideal gas constant, A is the pre-exponential factor and K (q_e /C_e) is the equilibrium constant [29,30].

To evaluate the effectiveness of the adsorbent in real matrices and to demonstrate the effect of interfering ions, wastewater samples were collected from a municipal wastewater treatment facility Istanbul European side, Türkiye. The wastewater samples were subjected to coarse and 0.45 µm membrane filtration and then spiked with CR standard solution at concentrations of 10, 30, and 50 mg/L. The optimized adsorption parameters were used to apply the same adsorption process to remove CR from real wastewater samples, and the results are presented as % removal. Wastewater samples were collected from, filtered to remove suspended particulates, and stored at 4 °C until further analysis.

3. Results and discussion

3.1. FTIR characterization of Fe_3O_4@MPA Nanoparticles

The FT-IR spectrum of bare Fe_3O_4 nanoparticles (Fig. 1) demonstrates a prominent absorption band at 543 cm^{-1}, indicative of Fe–O stretching vibrations within the magnetite spinel structure, thereby confirming the crystalline nature of the magnetic core. Following the functionalization with 2-mercaptopropionic acid (MPA), new absorption bands become apparent, signifying effective surface modification. Bands at 1591 cm^{-1} and 1537 cm^{-1} are attributed to asymmetric and symmetric carboxylate (-COO^-) stretching vibrations, while bands at 1451 cm^{-1} and 1405 cm^{-1} correspond to CH_2 bending and COO^- deformation modes. Peaks observed at 1271, 1207, and 1071 cm^{-1} are ascribed to C–O stretching and C–C skeletal vibrations of the MPA ligand. The emergence of these functional bands correlates with a decrease in intensity of the Fe–O peak at 543 cm^{-1}, indicating surface coverage by the organic modifier [31].

The adsorption of CR onto Fe_3O_4@MPA does not result in the emergence of new absorption bands, indicating that the dye is adsorbed through non-covalent interactions rather than the formation of new chemical bonds (Fig. 1). The majority of existing peaks, at 1591, 1537, 1451, 1207, 1071 cm^{-1}, and particularly at 543 cm^{-1}, which is indicative of Fe-O stretching, exhibit a significant increase in % transmittance, indicating their probable role in the adsorption mechanism.

The observed changes indicate the presence of electrostatic interactions, hydrogen bonding, and π-π stacking between the CR molecules and the functional groups on the MPA-modified surface. The observed decrease in Fe-O band intensity and the shift of the band at 543 cm^{-1} to 551 cm^{-1} prove that CR adsorption occurs on the surface (Fig. 1). The FT-IR spectral evolution indicates the successful functionalization of Fe_3O_4 with MPA and the subsequent physical adsorption of CR through surface-mediated interactions.

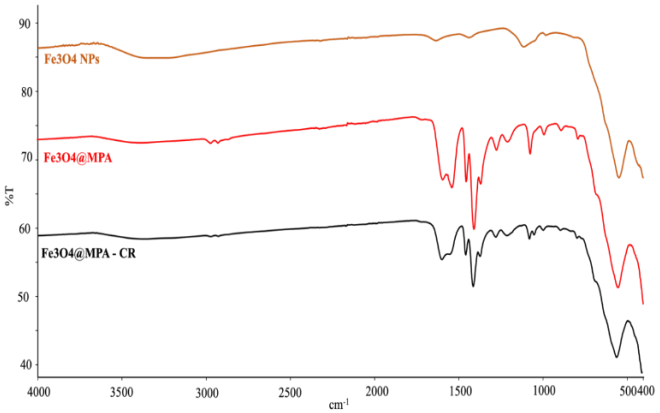

Figure 1. FTIR spectrum of nanoparticle, Fe_3O_4@MPA and Fe_3O_4@MPA-CR

3.2. Effect of pH on Congo Red adsorption

The adsorption performance of Fe_3O_4@MPA was investigated across a wide pH range (4–9), and the results revealed only minor differences in adsorption capacities (Fig. 2). Notably, the adsorption capacity at natural pH (q_e = 18.71 mg/g) was comparable to those obtained at the optimal pH values (pH 9, q_e = 19.03 mg/g). Given these minimal variations, further experiments were carried out without adjusting the solution pH. This strategy not only simplifies the adsorption process but also reduces the need for additional chemical reagents, improving the environmental and economic feasibility of the application. Similar approaches have been adopted in the literature.

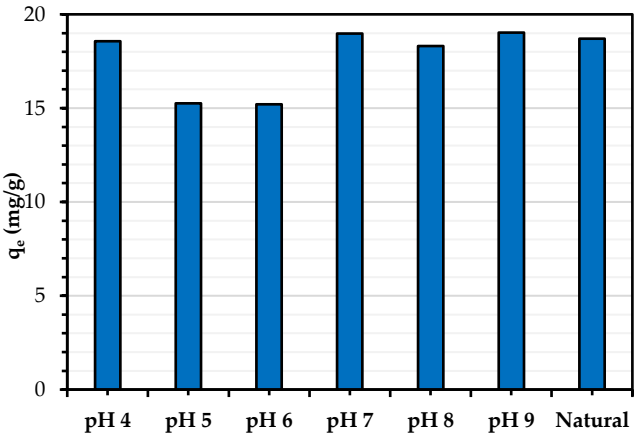

Figure 2. Effect of pH value on the CR adsorption (30 mg/L initial concentration, 10 mg Fe_3O_4@MPA, 2 hours contact time, at 25 °C)

For instance, Deng et al. (2022) [32] showed that Fe_3O_4 nanoparticles effectively removed Congo Red under ambient pH conditions without any performance loss. Studies by Zhu et al. (2011) [33] and Wang et al. (2012) [34] similarly concluded that Fe_3O_4-based adsorbents operate efficiently in unadjusted, near-neutral pH, supporting real-world applicability.

3.3. Adsorption isotherms

To evaluate the interaction mechanism between CR molecules and the surface of Fe_3O_4@MPA nanocomposite, equilibrium adsorption data were fitted to four commonly used isotherm models: The Langmuir, Freundlich, Temkin, and Dubinin–Radushkevich (D–R) methods were used. Adsorption capacities at equilibrium concentrations after 2 hours are given in Fig. 3.

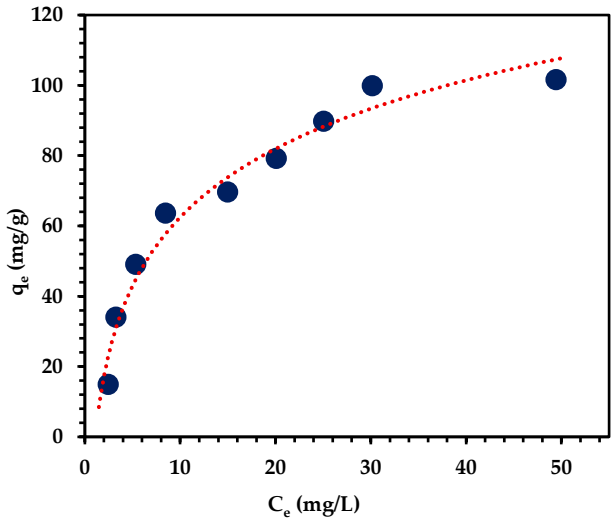

Figure 3. Adsorption capacities at equilibrium concentrations (30 mg/L initial concentration, 5 mg Fe_3O_4@MPA, 200 rpm, 2 hours contact time)

Adsorption experiments conducted at initial dye concentrations ranging from 20 to 100 milligrams per liter for 120 minutes and the isotherm models fitted data shown at Fig. 4. Among the evaluated models, the Langmuir isotherm demonstrated the optimal correspondence to the experimental data, exhibiting an elevated correlation coefficient, R^2=0.9901. The maximum adsorption capacity (q_m) was calculated to be 120.48 milligrams per gram (mg/g), and the Langmuir constant (K_L) was determined to be 0.1176 liters per milligram (L/mg). This finding indicates that the adsorption of CR onto Fe_3O_4@MPA occurs on a homogeneous surface via monolayer coverage, with minimal interaction between adsorbed dye molecules. This behavior is consistent with the findings of other studies involving thiol- and carboxyl-functionalized magnetic nanomaterials, which have been utilized for the removal of anionic dyes [35,36].

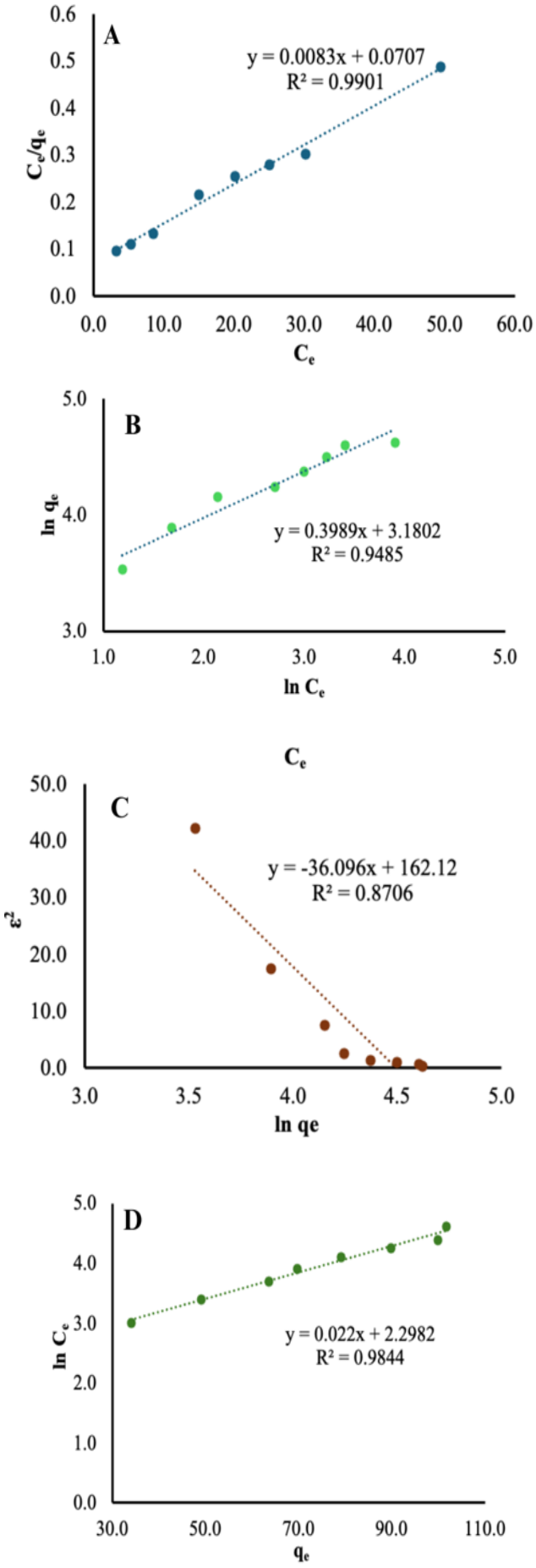

Figure 4. Isotherm plots CR adsorption on Fe_2O_4@MPA, A) Langmuir B) Freundlich C) D-R D) Temkin (25 °C, 10 mL volume, 5 mg Fe_3O_4@MPA adsorbent, 200 rpm, 2 hours)

In the Freundlich isotherm, which describes multilayer and heterogeneous adsorption, a moderate fit was yielded with an R^2 value of 0.9485. The constants K_F and n were found to be 24.05 and 2.51, respectively. The value of n>1 indicates favorable adsorption; however, the lower R^2 suggests that surface heterogeneity was not the dominant mechanism in this system.

The Temkin model also fit the data well (R^2 = 0.9844), suggesting moderate interactions between the dye and the adsorbent as well as uniform binding energy distribution up to a certain limit. The constants calculated were B=45.45 J/mol and A=9.9665 L/g.

In the D–R model, the theoretical monolayer capacity was q_m=89.17 mg/g, and the mean adsorption energy E=4.24 kJ/mol. The relatively low value of E shows typical for physical adsorption (which generally has E<8 kJ/mol) [19].

As can be seen in the adsorption isotherm parameters presented in Table 2, the results strongly support the applicability of the Langmuir model to explain the adsorption behavior of CR on Fe_3O_4@MPA nanoparticles. This indicates that single-layer, site-specific interactions dominate the process.

Table 2. Isotherm parameters obtained from Langmuir, Freundlich, Temkin, and Dubinin–Radushkevich models for CR adsorption.

Model	Parameters	R^2
Langmuir	q_m = 120.48 mg/g K_L = 0.1176 L/mg	0.9901
Freundlich	K_F= 24.05 n = 2.51	0.9485
Temkin	B= 45.45 J/mol A= 9.9665 L/g	0.9844
Dubinin–Radushkevich (D-R)	q_m = 89.17 mg/g, β = 0.0277 mol²/kJ² E = 4.24 kJ/mol	0.8706

3.4. Adsorption kinetics

The graph of the change in adsorption capacity with temperature in CR solutions with 50 mg/L initial concentration is shown in Fig. 5. The kinetic evaluation (Table 3) of Congo Red adsorption onto Fe_3O_4@MPA revealed a temperature-dependent transition in the adsorption mechanism. At lower temperatures, the pseudo-first order kinetic model provided a better fit, as reflected by a higher correlation coefficient (R^2 = 0.9504). However, as the temperature increased, particularly at 323 K and 333 K, the pseudo-second order model became dominant, with R^2 values as high as 0.9942 and 0.9922, respectively. This shift suggests that chemisorption mechanisms-which involve stronger, more specific interactions-become more significant at elevated temperatures.

These findings align with earlier studies reporting pseudo-second-order kinetics for the adsorption of anionic dyes onto functionalized magnetic nanoparticles, particularly in systems where surface complexation plays a significant role.

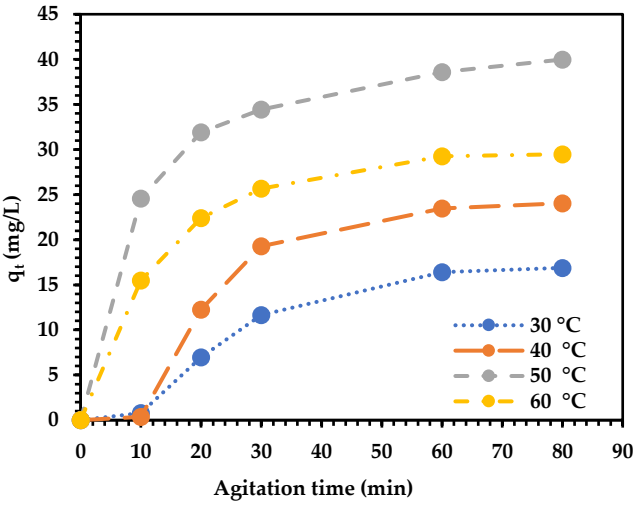

Figure 5. The effect of agitation time on adsorption capacity at different temperature (50 mg/L initial concentration, 10 mg Fe_3O_4@MPA, 200 rpm)

Table 3. Pseudo-first order and pseudo-second order kinetic parameters for CR (50 ppm initial concentration, 10 mg Fe_3O_4@MPA, 200 rpm)

T (K)	Pseudo-First Order			Pseudo-Second Order		
	k_1	q_e	R^2	k_2	q_e	R^2
303.15	0.063	26.311	0.9504	0.0031	19.6850	0.8490
313.15	0.007	34.960	0.9704	0.0038	26.4550	0.9346
323.15	0.053	29.595	0.9694	0.0076	40.8163	0.9942
333.15	0.081	33.478	0.9920	0.0090	30.4878	0.9922

These findings align well with existing studies in the literature. For instance, Zhu et al. (2011) reported that Congo Red adsorption onto magnetic cellulose/Fe_3O_4 composites follows pseudo-second-order kinetics, indicating chemical bonding as the rate-controlling step [33]. Moreover, Pietrzyk et al. (2022), who demonstrated excellent CR adsorption performance using Zn-doped Fe_3O_4 nanoparticles, highlighting second-order kinetics as the more accurate descriptor [37].

Considering these results and comparative literature, it can be confidently concluded that Fe_3O_4@MPA exhibits a kinetic transition from physical to chemical adsorption with increasing temperature, and that pseudo-second-order kinetics provides the most accurate description of the overall process at elevated temperatures.

3.5. Thermodynamic analysis

A van't Hoff plot ($\ln K_c$ vs 1/T) was used to determine the enthalpy (ΔH°) and entropy (ΔS°) changes. The results are presented in Table 4. All ΔG° values were negative, indicating a spontaneous adsorption process at all temperatures. Furthermore, the spontaneity increased slightly with temperature, suggesting that higher thermal energy facilitates the adsorption interaction.

Table 4. Thermodynamic parameters for CR adsorption onto Fe_3O_4@MPA nanoparticles at various temperatures

Temp. (°C)	Temp. (K)	Kc	ΔG° (kJ/mol)	ΔH° (kJ/mol)	ΔS° (kJ/mol·K)
30	303.15	1.464	–0.96	6.92	0.029
40	313.15	4.000	–3.61		
50	323.15	2.491	–2.45		
60	333.15	2.203	–2.19		

The enthalpy change (ΔH°=+6.92 kJ/mol) indicates that the process is endothermic, requiring energy input to proceed, which is typical for chemisorption. The positive entropy change (ΔS°=+0.029 kJ/mol·K) reflects increased randomness at the solid–solution interface during dye uptake, likely due to desolvation of CR molecules and increased mobility upon adsorption.

Although the correlation coefficient from the van't Hoff plot was relatively low ($R^2 = 0.066$), this is attributed to the estimation-based C_e values rather than to thermodynamic inconsistency. Overall, the results suggest a favorable, spontaneous, and endothermic chemisorption process, in agreement with other CR adsorption studies using functionalized magnetic nanomaterials or low-cost organic adsorbents [38].

3.6. Real matrix application

Solutions spiked with CR standard solution at concentrations of 10, 30, and 50 mg/L were subjected to the adsorption process under optimum adsorption conditions, and the % removal efficiency is shown in Fig. 6. The maximum adsorption efficiency was 60% in a 10 mg/L solution, indicating that the application of the method to real samples has a limited effect on the adsorption efficiency.

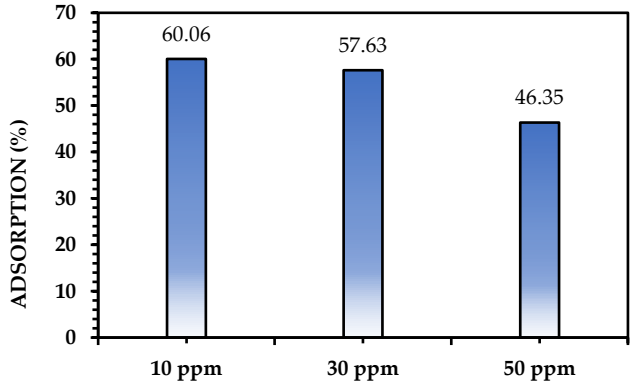

Figure 6. Adsorption efficiency (Removal, %) on real matrix

3.7. Comparison of adsorbent capacities

Table 5 comparisons of Congo Red adsorption properties of some magnetic and activated carbon-based adsorbents in the literature. As can be seen, the synthesized Fe_3O_4@MPA and the method developed with this adsorbent have good adsorption capacity compared to similar adsorbents in the literature.

Table 5. Adsorption capacity comparison table

Material	q_{max} (mg/g)	Best Isotherm	Best Kinetic Model	Ref.
$MnFe_2O_4$@Cel-g-p(AA-DMC)	60.2	Freundlich	Pseudo-second order	[39]
Magnetic iron oxide/kaolinite	45.6	Langmuir	Intraparticle diffusion model	[40]
Magnetic Chitosan	727.8	Freundlich	Pseudo-second order	[41]
Fe_3O_4@SiO_2-NH_2	24	Langmuir	Pseudo-second order	[42]
Fe_3O_4@Starch-acrilic acid	31.8	Langmuir	Pseudo-second order	[43]
Fe_3O_4/NiO	210.78	Langmuir	Pseudo-second order	[44]
m-Cell/Fe_3O_4 /ACCs	66.09	Langmuir	Pseudo-second order	[38]
Fe_3O_4@BTCA	630	Langmuir	Pseudo-second order	[45]
Lemon Peel-Fe_3O_4	16.28	Langmuir	Pseudo-second order	[46]
Fe_3O_4@MPA	120.48	Langmuir	Pseudo-second order	This study

4. Conclusion

In this study, Fe_3O_4 magnetic nanoparticles underwent a successful modification process with 2-mercaptopropionic acid, subsequently employed as an effective adsorbent for the elimination of CR dye from aqueous solutions. It has been suggested that the modified surface is conducive to adsorption in the presence of functional groups such as -SH and -COOH, and that these groups interact strongly with anionic dye molecules. Batch adsorption experiments showed that the adsorption efficiency was not significantly affected by pH and therefore, adsorption under natural pH conditions could be carried out cost-effectively and with less chemical use. The Langmuir isotherm model provided the most accurate description of the equilibrium data, indicating monolayer adsorption on a homogeneous surface, with a maximum adsorption capacity of 120.48 mg/g. The application of the Freundlich, Temkin, and Dubinin–Radushkevich models yielded ancillary insights into aspects related to surface energetics and adsorptive behavior. Kinetic modeling revealed that the pseudo-second order model provided an optimal fit to the experimental governed by chemisorption, a phenomenon characterized by valency forces. The spontaneous and endothermic nature of the adsorption process was confirmed by thermodynamic analysis, with negative ΔG°, positive ΔH° (6.92 kJ/mol), and positive ΔS° (0.029 kJ/mol.K) being observed. These results suggest an increase in randomness and molecular mobility at the solid–liquid interface during the uptake process. It was shown that the applied adsorbent and the developed method were affected by environmental factors to a limited extent in the adsorption of CR spiked into real wastewater samples. Overall, the Fe_3O_4@MPA

nanocomposite demonstrated strong potential as a low-cost, magnetically separable adsorbent for CR removal from wastewater. The material's high efficiency, stability, and functional properties make it promising for further development in wastewater treatment technologies.

Acknowledgements

The author gratefully acknowledges Büşra Şahin Kurt and Mehmet Enes Tezçakar for their valuable assistance and Nursu Aylin Kasa and Selim Gürsoy for their critical review of the manuscript.

References

[1] S.I. Siddiqui, E.S. Allehyani, S.A. Al-Harbi, Z. Hasan, M.A. Abomuti, H.K. Rajor, S. Oh, Investigation of Congo Red Toxicity towards Different Living Organisms: A Review, Processes, 11, 2023, 807.

[2] Y. Su, Y. Wang, L. Ding, Y. Chen, D. Song, An innovative and efficient strategy for removing Congo red using magnetic hollow Zn/Co zeolitic imidazolate framework composite, Environ Res, 264, 2025, 120399.

[3] A.K. Verma, R.R. Dash, P. Bhunia, A review on chemical coagulation/flocculation technologies for removal of colour from textile wastewaters, J Environ Manage, 2012, 93, 154–168.

[4] D. Mansour, E. Alblawi, A.K.D. Alsukaibi, B. Al Shammari, Removal of Congo red dye by electrochemical advanced oxidation process: optimization, degradation pathways, and mineralization, Sustain Water Resour Manag, 10, 2024, 41.

[5] J. Cevallos-Mendoza, C.G. Amorim, J.M. Rodríguez-Díaz, M. Montenegro, Removal of Contaminants from Water by Membrane Filtration: A Review, Membranes, 12, 2022, 570. v

[6] V. Vignesh, G. Shanmugam, Removal and recovery of hazardous congo red from aqueous environment by selective natural amino acids in simple processes, Process Biochemistry, 2023, 127, 99–111.

[7] S. Velusamy, A. Roy, S. Sundaram, T.K. Mallick, A Review on Heavy Metal Ions and Containing Dyes Removal Through Graphene Oxide-Based Adsorption Strategies for Textile Wastewater Treatment, The Chemical Record, 21, 2021, 1570.

[8] M. Harja, N. Lupu, H. Chiriac, D.D. Herea, G. Buema, Studies on the Removal of Congo Red Dye by an Adsorbent Based on Fly-Ash@Fe_3O_4 Mixture, Magnetochemistry 8, 2022, 125.

[9] N. Alsawaftah, W. Abuwatfa, N. Darwish, G. Husseini, A Comprehensive Review on Membrane Fouling: Mathematical Modelling, Prediction, Diagnosis, and Mitigation, Water, 13, 2021, 1327.

[10] M. Abbas, M. Trari, Mass transfer process in the removal of Congo Red (CR) onto Natural Clay (NC): Kinetic, isotherm modeling, and thermodynamic study, Journal of Water and Climate Change, 2023, 14, 2755–2772.

[11] A.M. Badran, U. Utra, N.S. Yussof, M.J.K. Bashir, Advancements in Adsorption Techniques for Sustainable Water Purification: A Focus on Lead Removal, Separations, 10, 2023, 565.

[12] S. Muthu Prabhu, N.R. Rane, X. Li, S.V. Otari, S.D. Girawale, A.R. Palake, K.M. Kodam, Y.K. Park, Y.H. Ha, K.K. Yadav, M.A. Khan, B.H. Jeon, Magnetic nanostructured adsorbents for water treatment: Structure-property relationships, chemistry of interactions, and lab-to-industry integration, Chemical Engineering Journal 468, 143474, 2023.

[13] N. Zhu, H. Ji, P. Yu, J. Niu, M.U. Farooq, M.W. Akram, I.O. Udego, H. Li, X. Niu, Surface Modification of Magnetic Iron Oxide Nanoparticles, Nanomaterials 8, 810, 2018.

[14] B. Sabzi Dizajyekan, A. Jafari, M. Vafaie-Sefti, R. Saber, Z. Fakhroueian, Preparation of stable colloidal dispersion of surface modified Fe3O4 nanoparticles for magnetic heating applications, Sci Rep, 14, 2024, 1296.

[15] P. Pączkowski, B. Gawdzik, Studies on Preparation, Characterization and Application of Porous Functionalized Glycidyl Methacrylate-Based Microspheres, Materials, 14, 2021, 1438.

[16] D. Hanaor, M. Michelazzi, C. Leonelli, C.C. Sorrell, The effects of carboxylic acids on the aqueous dispersion and electrophoretic deposition of ZrO2, J Eur Ceram Soc, 2012, 32, 235–244.

[17] R. Valenzuela, M.C. Fuentes, C. Parra, J. Baeza, N. Duran, S.K. Sharma, M. Knobel, J. Freer, Influence of stirring velocity on the synthesis of magnetite nanoparticles (Fe3O4) by the co-precipitation method, J Alloys Compd, 2009, 488, 227–231.

[18] K.L. Muedi, V. Masindi, J.P. Maree, N. Haneklaus, H.G. Brink, Effective Adsorption of Congo Red from Aqueous Solution Using Fe/Al Di-Metal Nanostructured Composite Synthesised from Fe(III) and Al(III) Recovered from Real Acid Mine Drainage, Nanomaterials, 12, 2022, 776.

[19] Ü.C. Erim, M. Gülfen, A.O. Aydın, Synthesis and selective Au(III) adsorption properties of poly(2-aminothiophenol) chelating polymer: equilibrium, kinetics and thermodynamics, International Journal of Environmental Science and Technology, 2025, 22, 4307-4320.

[20] Y.S. Ho, G. McKay, A comparison of chemisorption kinetic models applied to pollutant removal on various sorbents, Process Safety and Environmental Protection, 1998, 76, 332–340.

[21] M.A. Al-Ghouti, M.A.M. Khraisheh, M.N. Ahmad, S.J. Allen, Adsorption behavior of methylene blue onto Jordanian diatomite: A kinetic study, J Hazard Mater, 2009, 165, 589-598.

[22] N. Öztürk, D. Kavak, Adsorption of boron from aqueous solutions using fly ash: Batch and column studies, J Hazard Mater, 2005, 127, 81–88.

[23] Ü.C. Erim, M. Gülfen, A.O. Aydın, Separation of gold(III) ions by 1,8-diaminonaphthalene-formaldehyde chelating polymer, Hydrometallurgy, 2013, 134, 87–95.

[24] H.S. Kusuma, D.E.C. Jaya, G.I. Al Lantip, D.K. Afifah, A.C. Kirani, M. Mahfud, H. Darmokoesoemo, A.N. Amenaghawon, T.A. Kurniawan, Theoretical perspectives and recent advances in palm-based adsorbents for sustainable heavy metal removal from aqueous systems, Desalination Water Treat, 323, 2025, 101315.

[25] A. Çiçekçi, F. Sevim, M. Sevim, E. Kavcı. Adsorption Capacity, Reaction Kinetics and Thermodynamic Studies on Ni(II) Removal with GO@Fe_3O_4@Pluronic-F68 Nanocomposite, Polymers, 17, 2025, 2141.

[26] K.E. Alsamhary, Optimizing the process conditions for the biosorption of chromium (VI) by Bacillus subtilis in artificial wastewater, Electronic Journal of Biotechnology, 2025, 6, 22-38.

[27] T. Turna, A. Solmaz, A. Baran, Rapid adsorption of methylene blue by synthesizing zinc oxide nanoparticles from Ocimum basilicum L. waste, Int J Environ Sci Technol, 2025, 22, 10049–10066.

[28] P. Sethi, S. Basu, S. Barman, Innovative CuBTC/gC_3N_4 materials for tetracycline mitigation: adsorption, photocatalysis, and mechanistic perspectives, New Journal of Chemistry, 2025, 49, 8454-8471.

[29] E. Birinci, M. Gülfen, A.O. Aydın, Separation and recovery of palladium(II) from base metal ions by melamine–formaldehyde–thiourea (MFT) chelating resin, Hydrometallurgy, 2009, 95, 15–21.

[30] L. Tofan, I. Bunia, C. Paduraru, C. Teodosiu, Synthesis, characterization and experimental assessment of a novel functionalized macroporous acrylic copolymer for gold

separation from wastewater, Process Saf Environ Prot, 2017, 106, 150–162.
[31] L. Wang, L.M. Housel, D.C. Bock, A. Abraham, M.R. Dunkin, A.H. McCarthy, Q. Wu, A. Kiss, J. Thieme, E.S. Takeuchi, A.C. Marschilok, K.J. Takeuchi, Deliberate Modification of Fe3O4 Anode Surface Chemistry: Impact on Electrochemistry, ACS Appl Mater Interfaces, 2019, 11, 19920–19932.
[32] Q. Deng, X. Wang, M. Shao, L. Fang, X. Zhao, J. Xu, X. Wang, Synthesis of chitosan-modified magnetic metal-organic framework and its adsorption of Congo red and antibacterial activity, Microporous and Mesoporous Materials, 342, 2022, 112042.
[33] H.Y. Zhu, Y.Q. Fu, R. Jiang, J.H. Jiang, L. Xiao, G.M. Zeng, S.L. Zhao, Y. Wang, Adsorption removal of congo red onto magnetic cellulose/Fe3O4/activated carbon composite: Equilibrium, kinetic and thermodynamic studies, Chemical Engineering Journal, 2011, 173, 494–502.
[34] L. Wang, J. Li, Y. Wang, L. Zhao, Q. Jiang, Adsorption capability for Congo red on nanocrystalline MFe2O4 (M = Mn, Fe, Co, Ni) spinel ferrites, Chemical Engineering Journal, 2012, 181–182, 72–79.
[35] S. Laurent, D. Forge, M. Port, A. Roch, C. Robic, L.V. Elst, R.N. Muller, Magnetic iron oxide nanoparticles: Synthesis, stabilization, vectorization, physicochemical characterizations and biological applications, Chem Rev, 2008, 108, 2064–2110.
[36] C.T. Yavuz, J.T. Mayo, W.W. Yu, A. Prakash, J.C. Falkner, S. Yean, L. Cong, H.J. Shipley, A. Kan, M. Tomson, D. Natelson, V.L. Colvin, Low-field magnetic separation of monodisperse Fe3O4 nanocrystals, Science, 2006, 314, 964–967.
[37] P. Pietrzyk, N.T. Phuong, S.J. Olusegun, N.H. Nam, D.T.M. Thanh, M. Giersig, P. Krysiński, M. Osial, Congo Red removal with superparamagnetic iron-oxide nanoparticles doped with zinc, Magnetochemistry, 8, 2022, 91.
[38] H.Y. Zhu, Y.Q. Fu, R. Jiang, J.H. Jiang, L. Xiao, G.M. Zeng, S.L. Zhao, Y. Wang, Adsorption removal of congo red onto magnetic cellulose/Fe3O4/activated carbon composite: Equilibrium, kinetic and thermodynamic studies, Chemical Engineering Journal, 2011, 173, 494–502.
[39] C. Ling, D. Yimin, L. Qi, F. Chengqian, W. Zhiheng, L. Yaqi, C. Ling, L. Bo, Z. Yue-fei, L. Yan, W. Li, Fabrication of magnetic targeted cellulose/poly (acrylic acid-co-2-methacryloyloxyethyl trimethylammonium chloride) composites for adsorbing Congo red dye from aqueous solution, J Mater Sci: Mater Electron, 2022, 33, 5750–5762.
[40] N. Mahmud, A. Benamor, Magnetic Iron Oxide Kaolinite Nanocomposite for Effective Removal of Congo Red Dye: Adsorption, Kinetics, and Thermodynamics Studies. Water Conserv Sci Eng, 8, 2023, 35.
[41] H. Wang, W. Luo, R. Guo, D. Li, B. Xue, Effective adsorption of Congo red dye by magnetic chitosan prepared by solvent-free ball milling, Mater Chem Phys, 292, 2022, 126857.
[42] C.R. Lin, O.S. Ivanova, D.A. Petrov, A.E. Sokolov, Y.Z. Chen, M.A. Gerasimova, S.M. Zharkov, Y.T. Tseng, N.P. Shestakov, I.S. Edelman, Amino-Functionalized Fe3O4@SiO2 Core-Shell Magnetic Nanoparticles for Dye Adsorption, Nanomaterials 11, 2021, 2371.
[43] A. Saberi, E. Alipour, M. Sadeghi, Superabsorbent magnetic Fe3O4-based starch-poly (acrylic acid) nanocomposite hydrogel for efficient removal of dyes and heavy metal ions from water, J Polym Res, 26, 2019, 271.
[44] P. Koohi, A. Rahbar-kelishami, H. Shayesteh, Efficient removal of congo red dye using Fe3O4/NiO nanocomposite: Synthesis and characterization, Environ Technol Innov, 23, 2021, 101559.
[45] S. Chatterjee, N. Guha, S. Krishnan, A.K. Singh, P. Mathur, D.K. Rai, Selective and Recyclable Congo Red Dye Adsorption by Spherical Fe3O4 Nanoparticles Functionalized with 1,2,4,5-Benzenetetracarboxylic Acid, Sci Rep, 10, 2020, 111.
[46] A.O. Nasser, S.L. Kareem, Removal of Congo red from aqueous solution using lemon peel-Fe3O4 nanocomposite adsorbent, Biomass Convers Biorefin, 2024, 14, 23183–23193.